

M.Y. GOULKOV¹
T. GRANZOW²
U. DÖRFLER²
T. WOIKE²
M. IMLAU^{3,✉}
R. PANKRATH³

Study of beam-fanning hysteresis in photorefractive SBN:Ce: light-induced and primary scattering as functions of polar structure

¹ Institute of Physics, National Academy of Sciences of Ukraine, Science Ave 46, 03650 Kiev-39, Ukraine
² Institut für Mineralogie, Universität zu Köln, Zülpicher Str. 49b, 50674 Köln, Germany
³ Fachbereich Physik, Universität Osnabrück, 49069 Osnabrück, Germany

Received: 27 August 2002/Revised version: 19 December 2002
Published online: 26 March 2003 • © Springer-Verlag 2003

ABSTRACT We study light-induced scattering (beam-fanning) in the photorefractive crystal SBN:Ce as a function of the polar structure of the crystal. The spatial structure of the beam-fanning is measured at different externally applied electric fields, and an optical hysteresis is found in the scattering. It is shown that the scattering hysteresis results from a polarization hysteresis typical for ferroelectrics in the polar phase. New information about primary scattering in SBN is obtained, and a corresponding model of its origin is proposed. It is shown that the intensity and angular distribution of the primary scattering strongly depend on the polar structure of the crystal and can be affected by the subsequent action of an external field and coherent illumination.

PACS 42.65.Hw; 42.70.Mp; 77.80.Dj

1 Introduction

Cerium-doped $\text{Sr}_{0.61}\text{Ba}_{0.39}\text{Nb}_2\text{O}_6$ (SBN:Ce) possesses significant photorefractive properties [1, 2] in the ferroelectric phase, which make it possible to record a refractive index grating in this material using a pair of coherent light waves: the spatially periodic light pattern formed by the two waves induces a space-charge field E_{sc} , due to the diffusion of photoexcited electrons, which modulates the index of refraction via the linear electrooptic effect [3]. Beam coupling [4] on this photorefractive grating results in the enhancement of the intensity of one recording wave and the depletion of the other. Light-induced wide-angle polarization-isotropic scattering (usually known as beam-fanning [5]) always accompanies the propagation of a single extraordinary laser beam in SBN and is a result of the nonlinear coupling of scattered and transmitted parts of the laser beam (pump beam in the following). The pump beam is scattered on crystal imperfections, and the coherent seed scattering records refractive gratings with the pump beam. Mutual diffraction of the seed and pump waves on noisy gratings results in an enhancement of the light scattered in the direction of positive energy exchange and a corresponding partial depletion of the pump beam. The efficiency and direction of the energy exchange are related to

the macroscopic ferroelectric polarization in the crystal via the linear electrooptic coefficients. Thus, the macroscopic ferroelectric polarization defines the orientation in space and intensity of the light-induced scattering.

The spontaneous polarization P_s in SBN is attributed to the displacement of metal atoms from the oxygen planes along the four-fold axis of the NbO_6 octahedra [6]. To order ferroelectric domains in one direction, and thus to make the macroscopic polarization in SBN apparent, an as-grown sample has to be electrically poled by applying an external electric field. The displacement of the atoms in the niobium–oxygen octahedra also causes the distortion of the covalent Nb–O bonds in the octahedra and results in the linear electrooptic effect. The electrooptic effect in a single-domain SBN crystal depends on the temperature and strongly increases when the crystal approaches the phase transition temperature T_c [7]. SBN samples doped with 0.66 mol % of cerium exhibit a value of $T_c = 52^\circ\text{C}$ [8]. Hence, even slight heating should improve the photorefractive response in highly doped SBN:Ce. At the same time, unpoled SBN, which is characterized by a disordered polar structure, does not possess a linear electrooptic effect, and its nonlinear properties strongly differ from those in electrically poled samples.

The polar structure of a SBN crystal consists of domains of various dimensions from a few nm to hundreds of μm [9, 10] arising from crystal defects and inhomogeneities, which serve as nucleation centers during the phase transition from the high-temperature paraelectric phase to the low-temperature ferroelectric phase. Usually, local defects, disordered crystal planes, and dislocations are considered the most probable defects in SBN. Doping of SBN with cerium not only improves the photorefractive properties due to the incorporation of photorefractive Ce^{3+} centers on off-center Sr^{2+} sites [11], but also considerably increases the number density of defects. The spontaneous polarization P_s suffers changes as a result of these defects, and $\nabla \cdot P_s$ serves as a local depolarization field. The domains appear to minimize the energy associated with these local fields. The depolarization fields can be strong enough to screen some regions and to create domains oriented opposite to the average direction of P_s (so-called 180° -domains). Very high domain densities in the interior of SBN samples have been reported [12], much higher than in BaTiO_3 .

A great advantage of ferroelectrics in many applications is connected with the possibility of controlling the electric

✉ E-mail: mirco.imlau@uni-osnabrueck.de

polarization P_s via the external electric field E_o , which is usually illustrated by the well-known P – E hysteresis [13]. The macroscopic polarization reverses its direction when the external field exceeds the coercive field E_c . The hysteresis response of the domain structure should result in a corresponding hysteresis behavior of the photorefractive properties in SBN when external fields are applied. Optical hysteresis has already been revealed in two-beam coupling experiments with SBN [14–18], showing the dependence of the beam-coupling increment Γ on an external electric field (Γ – E hysteresis). We should point out that the principal difference between measurements of the optical hysteresis and classical P – E hysteresis measurements is the coherent illumination of the ferroelectric crystal during (or after) the application of the external electric field when the hysteresis is measured. In the P – E hysteresis measurements, where P_s is measured electrically, the sample is not optically illuminated. Due to the low dark conductivity, free electrons cannot play an important role in the compensation of the depolarization fields and therefore are not able to affect the formation of the domain structure. In the case of optical hysteresis measurements, when the crystal is necessarily illuminated by coherent light, a current of photoinduced electrons can be sufficient to modify the compensation conditions and to affect the domain structure.

In this paper, we concentrate our attention on the study of beam-fanning in SBN:Ce in externally applied fields. We report on the observation of optical hysteresis in the light-induced scattering in a $\text{Sr}_{0.61}\text{Ba}_{0.39}\text{Nb}_2\text{O}_6$:Ce single crystal and show that the scattering hysteresis is a result of the conventional P – E hysteresis. Examining the experimental results of the scattering hysteresis quantitatively, we obtain new information about the gain factor Γ and the seed scattering I_{s0} as functions of the external electric field. This allows us to discuss a simple model of the seed scattering in SBN and to analyze the effect of coherent illumination and external fields on the domain structure. We consider optical inhomogeneities induced by local electric fields on domain boundaries as sources of the seed scattering. The coherent illumination of the crystal leads to an additional charging of the domain boundaries and to an enhancement of the scattering centers. This model allows us to explain all features of the scattering hysteresis observed in the experiment. We also show that coherent illumination can either assist or hinder the process of domain inversion in SBN, depending on the conditions under which the optical irradiation and electric field are applied to the sample. We conclude that the successive action of coherent irradiation and the application of external fields improves the domain structure and increases the photorefractive properties of SBN, and also considerably enhances the number of scattering centers in the crystal volume.

2 Experimental setup

A single crystal of SBN doped with 0.66 mol % of cerium, grown at the congruently melting composition by the Czochralski technique, was cut into a rectangular parallelepiped with dimensions of $a \times b \times c = 5.65 \times 0.7 \times 2.75 \text{ mm}^3$. The sample was electrically poled by heating up to 140°C , applying an external electric field of 3.5 kV/cm along the c axis, and then slowly cooling back to room temperature

before removing the field. After the poling process, the crystal was placed in the experimental setup so that its polar c axis was initially oriented from the left to the right hand side of the sample as shown in Fig. 1 (the Cartesian z -vector was chosen to be oriented in the same direction).

The unexpanded beam of a He–Ne laser ($\lambda = 633 \text{ nm}$) served as the pump beam and was directed along the crystal normal onto the large (a – c)-face of the sample (see Fig. 1). An extraordinary light polarization was chosen. The beam intensity was adjusted to $I_p = 70 \text{ mW/cm}^2$. The beam diameter $d = 1.5 \text{ mm}$ was smaller than the input face of the sample and did not allow complete illumination of the sample. The absorption coefficient of the sample was measured to be 4 cm^{-1} at $\lambda = 633 \text{ nm}$, which is negligibly small.

The 2D pattern of light-induced scattering was usually observed on a screen (not shown in Fig. 1) placed behind the sample. To measure an angular intensity distribution in the scattering pattern, a photodetector (PD) was mounted on a motorized rotation stage at a distance of $L = 5.5 \text{ cm}$ behind the sample and made an exact half-circle around the sample when moving in the direction from negative to positive z . This allowed us to monitor the intensity distribution along the polar axis for scattering angles of $\theta_s = \pm 90^\circ$ measured in air. Negative and positive angles correspond to scattering in $-z$ and $+z$ direction, respectively. At $\theta_s = 0^\circ$, the photodetector crossed the pump beam behind the crystal. The photodetector aperture limited the apex angle of the measured light to 0.5° . The entire setup was placed within a black box (not shown in Fig. 1), with only a small opening for the entrance of the pump beam, to minimize the background noise due to external light sources.

To set and control the temperature, the crystal was mounted on a Peltier element. A temperature controller allowed adjustment of the temperature in the range $+10$ to $+150^\circ\text{C}$ with an absolute accuracy of 0.3°C .

To apply the external electric field E_o to the sample, the surfaces normal to the polar axis were covered with conducting silver paste and connected to a dc power supply. The necessary amplitude was established in steps of $\Delta E_o = 0.182 \text{ kV/cm}$, with a lag time of 2 s between steps. Fields applied in the same direction as during the poling procedure were considered as positive, while fields applied in the opposite direction were considered as negative.

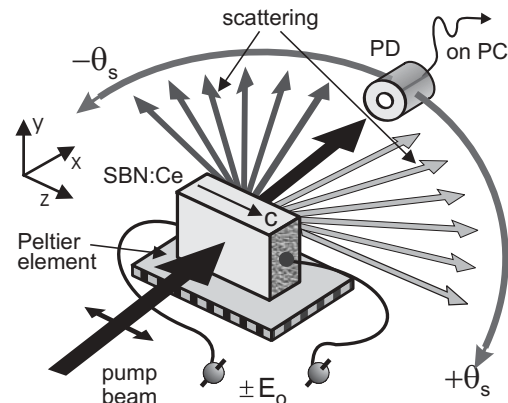


FIGURE 1 Schematic representation of the experimental set-up with SBN:Ce

Two procedures for applying the electric field were used.

Procedure 1. Application of an external field without illumination and subsequent illumination at zero-field: The external field E_0 was applied to the crystal without any illumination for a duration of 10 s, then it was switched off. After a relaxation time of 1–2 minutes, which is long enough to reach the steady state of the spontaneous polarization in SBN [19], the crystal was illuminated with the pump beam. The asymmetric scattering pattern was built up, and its angular distribution was investigated in the steady state.

Procedure 2. Application of the external field to a continuously illuminated crystal: The pump beam was turned on, then the external field was applied and raised to the amplitude E_0 . 10 minutes after the amplitude E_0 was reached, the measurement of the angular distribution of the scattering was started. The field remained applied during illumination. The crystal was illuminated, irrespective of whether the external field was applied or varied in amplitude.

3 Experimental results

During propagation through the SBN sample, the laser beam was fanned, yielding a spatially asymmetric polarization-isotropic scattering pattern (e-polarized scattering). The time necessary to achieve the stationary distribution of scattered light was about 10 minutes at the intensities used in the experiment. A typical beam-fanning pattern observed on the screen placed behind the crystal is shown in Fig. 2a. Note that the bright diffusive strip of scattered light is located on the left hand side of the pump beam in the negative direction of the c axis ($-c$ -direction).

Figure 2b shows three beam-fanning profiles measured with the same SBN sample at different temperatures for the case in which no external field was applied to the sample: curve 1 is for $T = 28^\circ\text{C}$ (ferroelectric phase), curve 2 is for $T = 52^\circ\text{C}$ ($T \approx T_c$) and curve 3 is for $T = 130^\circ\text{C}$ (paraelectric phase). The central intensity peak at $\theta_s = 0^\circ$ was formed by the transmitted pump beam (the shadowed area marks the angular interval over which the pump peak influences the scattering distribution). Results of temperature studies of the beam-fanning in SBN are presented in detail in [20], but since it is not a main subject of the current paper, we shall mention here only some basic properties particularly important for us now: 1) If SBN is in the ferroelectric phase, the scattering pattern is strongly asymmetric, and most of the scattered light is observed in the direction opposite to the c axis of the crystal (negative scattering angles θ_s in Fig. 2); 2) Due to a strong temperature dependence of the beam coupling process, heating the crystal up to $T_c = 52^\circ\text{C}$ significantly increases the total scattering intensity and at the same time makes the asymmetry of the angular light distribution more pronounced; 3) Because of the relaxor behavior of SBN [21, 22], quite strong light-induced scattering is observed even for $T > T_c$ due to the presence of polar clusters; 4) In the paraelectric phase at $T \gg T_c$, where polar clusters vanish and no beam-coupling is possible because the polar macrostructure is no longer present, only the weak seed scattering is observed. Due to the drastic changes in the domain structure at the phase transition, the seed scattering at 130°C differs from that at 28°C both in the total amount and in the angu-

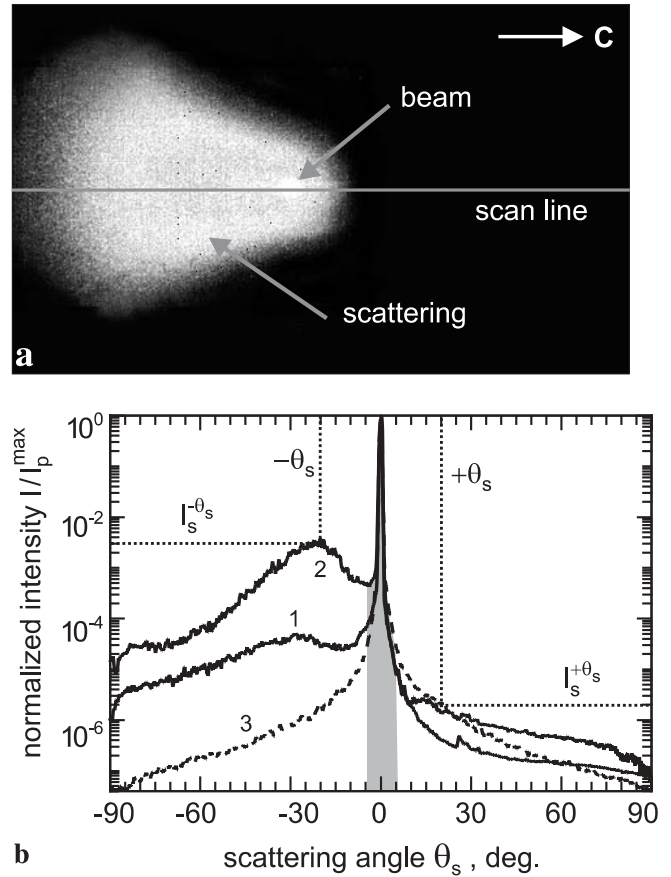


FIGURE 2 a Photo of the scattering pattern on the screen behind a SBN:Ce crystal at $T = 28^\circ\text{C}$. b Angular distributions of scattered light measured along the c axis at zero external field and different temperatures: $T = 28^\circ\text{C}$ (curve 1), $T = 52^\circ\text{C}$ (curve 2), and $T = 130^\circ\text{C}$ (curve 3). The central peak corresponds to the transmitted pump beam. The shadowed area displays the angular interval influenced by the transmitted pump beam

lar distribution. In order to obtain asymmetric scattering with a well-pronounced maximum, we set the crystal temperature to $T = 49^\circ\text{C}$. All results presented below were obtained for this particular temperature.

In the following, we consider the total scattering intensity I_s measured from angular profiles as the sum of the total scattering intensity I_- on the left hand side (the area under the experimental curve at negative scattering angles) and the total scattering intensity I_+ on the right hand side (the area under the experimental curve at positive scattering angles) from the central shadowed part of the angular profile: $I_s = I_- + I_+$. The central peak itself was excluded from the calculations in order to avoid a contribution from the transmitted part of the pump beam. We also introduce the coefficient $m_s = (I_- - I_+) / (I_- + I_+)$ as a parameter defining the spatial orientation of the scattering pattern. This coefficient is sensitive to changes in the spatial distribution of the scattered light and changes its sign when the beam-fanning reverses in space. The coefficient m_s is positive if the scattering is located primarily on the left hand side of the pump beam (initial orientation of the beam-fanning at $E_0 = 0$), and is negative if the scattering is spatially inverted and its maximum appears on the right hand side of the pump beam. This can happen if the orientation of the polar axis is inverted.

To study the influence of the external electric field on the light-induced scattering, we applied the field E_o to the SBN sample along the c axis.

Procedure 1. First, we used Procedure 1, where the processes of field application and illumination of the crystal are separated in time.

We started with $E_o = 0$ and gradually changed the field to the largest negative amplitude $E_o = -4$ kV/cm, then went in the opposite direction and approached the value $E_o = +4$ kV/cm before reducing the field back to zero. The electric field was changed in steps of 0.182 kV/cm. After each step of electric field application, a new scattering distribution developed and was measured. The five angular scans shown in Fig. 3 represent the most crucial points in the evolution of the scattering distribution. The curve in Fig. 3a corresponds to the beam-fanning with no applied field; the scattering distribution is characterized by the coefficient $m_s = 0.93$, while the normalized total scattering intensity is defined to be 1 here. When weak negative fields were applied to the sample, the scattering pattern remained almost unchanged, and m_s and I_s remained practically constant. Starting at a field of $E_o = -1.1$ kV/cm, the scattering sharply decreased in intensity and became more and more symmetric. The angular profile in Fig. 3b was measured after the field $E_o = -1.3$ kV/cm had been applied to the sample. The smallest coefficient $m_s = 0.16$ was measured after $E_o = -1.5$ kV/cm, indicating that this value is very close to the coercive field E_c . The corresponding intensity distribution (see Fig. 3c) is almost symmetric and looks very similar to that measured in the paraelectric phase (curve 3 in Fig. 2). The total scattering intensity after applying $E_o = -1.5$ kV/cm was smaller by a factor of 0.2 than the value measured at the starting point ($I_s^{E_o=0}$). Further increase of the electric field led to a switching of the scattering pattern from the $-z$ to the $+z$ direction. Correspondingly, the coefficient m_s became negative. If the negative field was increased further, the $-z$ -scattering continued to decrease, the $+z$ -scattering was strongly amplified, and the total scattering intensity increased. This evolution is illustrated by the following two curves: one was measured after $E_o = -1.8$ kV/cm was applied (Fig. 3d), the other was measured after $E_o = -4$ kV/cm was applied (Fig. 3e). The latter is characterized by the coefficient $m_s = -0.95$, and the total scattering intensity was 1.5 times stronger compared to the starting point with $E_o = 0$ kV/cm.

Figure 4a and b shows the electric field dependencies of the coefficient m_s and the scattering intensity I_s normalized relative to the zero-field intensity in more detail. The scattering profiles shown in Fig. 3 correspond to the part of the experimental results marked by filled circles on the curves in Figs. 4a and b. Arrows indicate the direction of the change of E_o during the experiment. It can be seen from Fig. 4a that when the external field went from -4 kV/cm to positive values, the coefficient m_s remained unchanged until a field of $E_o = +1.2$ kV/cm was exceeded. Then it reversed its sign back to positive and approached a value of $m_s = 0.96$, measured at $E_o = +4$ kV/cm. The value of E_o at which the m_s -curve crosses the abscissa is different for descending (left) and for ascending (right) parts of the scattering hysteresis. This allows us to evaluate the coercive field E_c to be 1.53 kV/cm and 1.22 kV/cm, respectively, if the external field is anti-

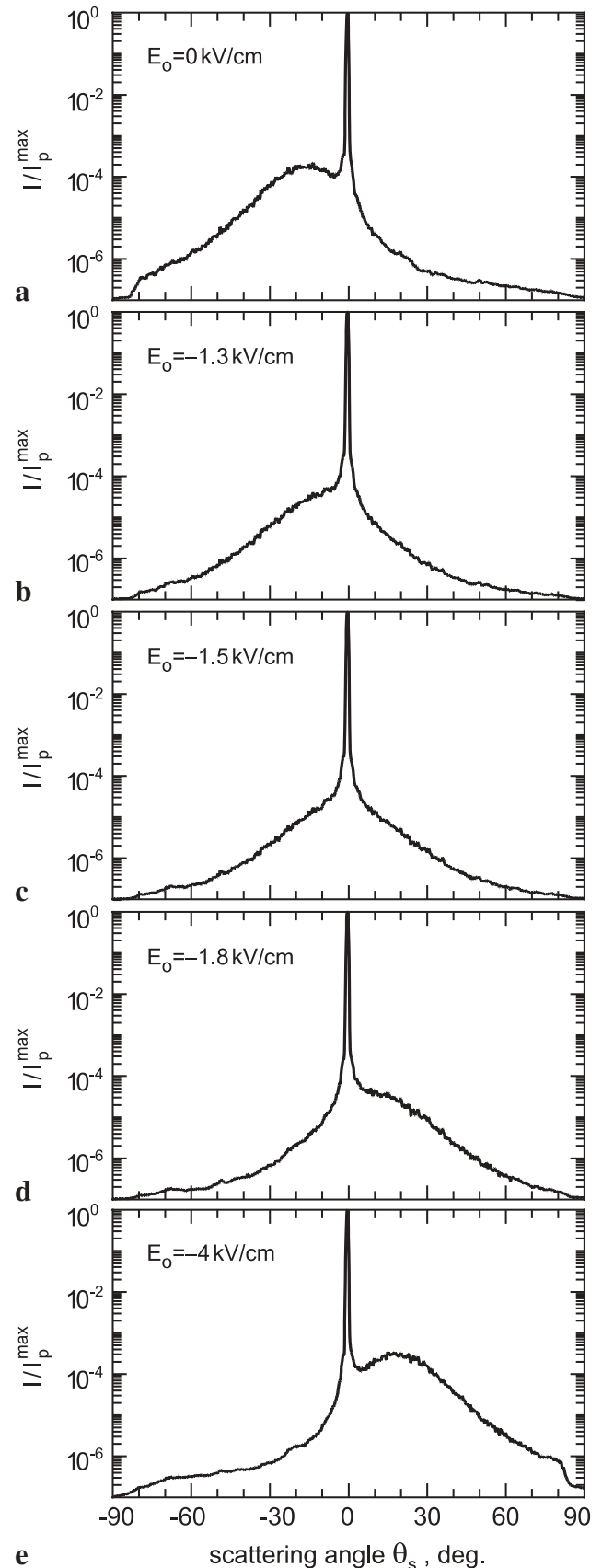


FIGURE 3 Angular distributions of scattering intensity at different external dc fields: **a** $E_o = 0$ kV/cm; **b** $E_o = -1.3$ kV/cm; **c** $E_o = -1.5$ kV/cm; **d** $E_o = -1.8$ kV/cm; **e** $E_o = -4$ kV/cm. The crystal temperature was $T = 49$ °C.

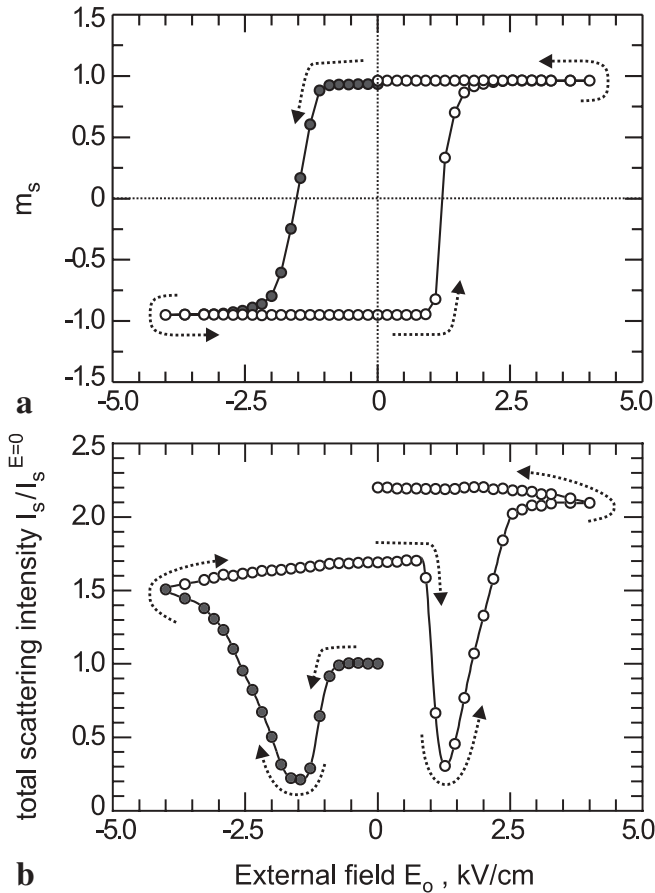


FIGURE 4 Results of a scattering hysteresis experiment with an external electric field E_0 applied with Procedure 1: **a** coefficient $m_s = (I_- - I_+) / (I_- + I_+)$ versus E_0 ; **b** total scattering intensity I_s (normalized relative to the zero-field scattering intensity) versus E_0 . Arrows shows how the field was changed

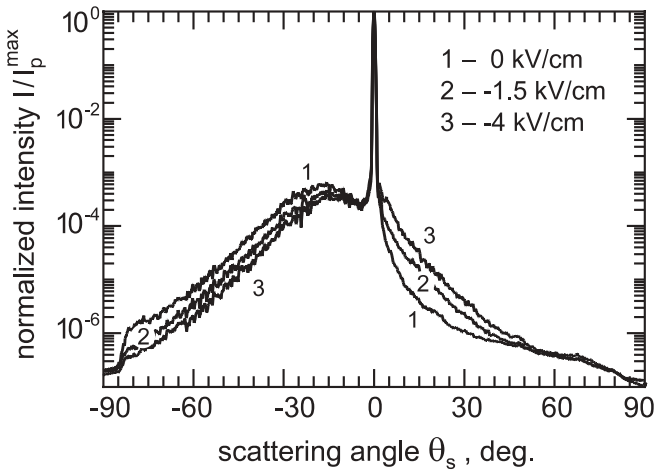


FIGURE 5 Angular distribution of scattering intensity at different external electric fields applied with Procedure 2: $E_0 = 0$ kV/cm (curve 1), $E_0 = -1.5$ kV/cm (curve 2), $E_0 = -4$ kV/cm (curve 3). The crystal temperature was $T = 49$ °C

parallel and parallel to the initial direction of P_s after the poling of the sample at high temperatures. At the same time, according to Fig. 4b, the total scattering intensity increased slightly at high negative fields (after $E_0 = -4$ kV/cm), saturated near zero field, then dropped into the next minimum at $E_0 \approx +1.3$ kV/cm. It then increased again at high positive

fields. When the external field was finally reduced to zero, the coefficient m_s remained nearly constant, and the total scattering intensity arrived at a value which was higher by a factor of 2.2 than that of the starting point. The hysteresis-like behavior of $m_s(E)$ indicates the ability of the beam-fanning to reverse its orientation in space perfectly when the external field is applied to the SBN sample using Procedure 1.

Procedure 2. The same experiment performed with procedure 2 (pump beam illuminates the crystal while the external field is applied) did not result in a scattering hysteresis. Scattering profiles measured at three principal values E_0 are shown in Fig. 5. The first curve corresponds to $E_0 = 0$ V/cm, the second curve corresponds to $E_0 = -1.5$ kV/cm and the third curve shows the results obtained at $E_0 = -4$ kV/cm. The direction of the polarization did not change.

4 Discussion

4.1 Basic photorefractive model of light-induced scattering in SBN

Wide-angle polarization-isotropic scattering from a single pump beam (beam-fanning) in SBN is a typical photorefractive phenomenon usually interpreted as being a result of nonlinear two-beam coupling between scattered and transmitted parts of the incident beam [5, 23].

To treat our experimental data, we restrict ourselves to a simplified photorefractive model and assume that:

- 1) in the absence of an external electric field, a diffusion of photocarriers dominates the charge transport in SBN, since the photovoltaic effect is extremely small in SBN:Ce [24] at the temperatures used in the experiment;
- 2) electrons are the major contributors to photoinduced currents [2], and the influence of positive charge carriers (holes) can be neglected;
- 3) an undepleted pump approximation [3, 25] can be used in the case of the comparatively weak light-induced scattering (see Fig. 3);
- 4) the absorption coefficient for SBN:Ce ($\alpha = 4$ cm $^{-1}$ at $\lambda = 633$ nm) can be approximated as zero in order to simplify the model equations and the numerical treatment of the experimental results.

The pump beam propagates in the crystal and is partially scattered by optical inhomogeneities and imperfections in the sample. This initial optical noise consists of plane seed waves propagating at different angles θ_s from the direction of the pump beam. The seed wave s interferes with the pump wave p and forms an elementary light pattern $I = I_0(1 + m \cos(\mathbf{K} \cdot \mathbf{r}))$ with a spatial period of $\Lambda = \lambda / (2 \sin \theta_s) = 2\pi / K$, where λ is the wavelength of the incident light, \mathbf{K} is the grating vector of the light modulation, $m = 2\sqrt{I_s \cdot I_p} / I_0$ is the modulation depth, and $I_0 = I_s + I_p$. Due to processes of thermal diffusion and drift in the external field (when the field is applied), photoexcited electrons migrate from bright to dark regions and yield the periodically modulated space-charge field $E_{sc}(\mathbf{r}) = m E_{sc}^0 \cos(\mathbf{K} \cdot \mathbf{r} + \Phi)$, where E_{sc}^0 is the amplitude of the spatially varying field and Φ its phase shift with respect to the incoming light interference pattern [3, 26]. In the case of SBN the phase shift is always exactly $\Phi = 90^\circ$ when there is

no external electric field ($E_o = 0$). In our experiment the externally applied electric field leads to a change of the phase shift Φ of up to 5%, which can be neglected. The increase of the space-charge field at the maximum field strength of $E_o = 4$ kV/cm is only 15% compared to zero field.

The linear electrooptic effect transfers the electric charge grating into a refractive index grating: $\Delta n(\mathbf{r}) = (\Delta n)_o \sin(\mathbf{K} \cdot \mathbf{r}) = -0.5r_{\text{eff}} n_{\text{eff}}^3 E_{\text{sc}}^o \sin(\mathbf{K} \cdot \mathbf{r})$, where n_{eff} is the effective refractive index and r_{eff} is the effective electrooptic coefficient. The spatial $\Lambda/4$ -shift between the refractive grating and the light pattern causes an effective stationary energy exchange between pump and seed waves, resulting in an exponential change of the intensity of the seed wave: $I_s(d) = I_{s0} \exp(\Gamma d)$, where d is the crystal thickness, and the exponential increment $\Gamma = 4\pi(\Delta n)_o/\lambda \cos \theta_s$ is the gain coefficient describing the efficiency of the direct coupling between the p and s waves. When using the corresponding expression for the amplitude of the diffusion field [26] and taking into account the particular conditions of our experiment, the coupling coefficient Γ can be written for the beam fanning in SBN as

$$\Gamma = \mp \frac{2\pi n_e^3 r_{33}}{\lambda \cos \theta_s} \frac{k_B T}{e} \frac{K}{1 + (K/K_D)^2}, \quad (1)$$

where e is the elementary electric charge, k_B is Boltzmann's constant and T is the absolute temperature. The inverse Debye-screening length K_D is given by $K_D = \sqrt{e^2 N_{\text{eff}} \times \sqrt{1/(\epsilon_{33}\epsilon_o k_B T)}}$, where ϵ_{33} and ϵ_o are the dielectric constants of SBN and free space, respectively. The effective trap density N_{eff} has been measured to be $2.2 \times 10^{23} \text{ m}^{-3}$ for SBN doped with 0.66 mol% of cerium [27]. The sign of r_{33} has been measured to be positive [27, 28]. Hence, the scattering that propagates in the $-c$ -direction (positive Γ) is amplified, and that in the $+c$ -direction (negative Γ) is depleted, resulting in the strongly asymmetric scattering pattern shown in Fig. 2.

Here we have to note that the effect of the external electric field cannot be reduced only to small changes of E_{sc}^o and Φ values. High electric fields E_o larger than the coercive field E_c should result in a spatial inversion of the macroscopic polarization P_s of the sample and in a corresponding inversion of the sign of the gain coefficient Γ .

4.2 Light-induced scattering hysteresis

To explain a spatial switching of beam-fanning and the hysteresis-like behavior of the coefficient m_s in SBN under an external electric field, one should consider the correlation between the photorefractive effect and the spontaneous polarization of the crystal. The linear electrooptic coefficient r_{33} depends on the macroscopic polarization P_s through [29]

$$r_{33} = 2g_{33} P_s \epsilon_{33} \epsilon_o, \quad (2)$$

where g_{33} is the quadratic electrooptic coefficient. An inversion of the vector of the spontaneous polarization changes the sign of r_{33} in (2). This in turn causes a change of the sign of the gain factor Γ in (1), and results in the spatial inversion of the beam-fanning. SBN exhibits the smallest gain coefficient (down to $\Gamma \approx 0$) under the external field $E_o = E_c$, because the

macroscopic polarization here, and therefore the electrooptic coefficient, nearly vanishes due to the equal number of inverted and non-inverted domains in the crystal. This results in the reduction of the total scattering intensity and in the spatial symmetrization of the scattering pattern, as observed in the corresponding curve in Fig. 3c. As was mentioned in the experimental section, this curve looks similar to the one measured in the paraelectric phase (Fig. 2). The shape of the light profiles is symmetric. The difference is that, in the paraelectric phase, the domain structure is destroyed by high thermal energies, while in the low-temperature phase the cooperative interaction of domains is only compensated by the action of a negative external field $E_o = E_c$. However, this compensation does not remain at $E_o \neq E_c$. For $E_o \gg E_c$, the polar structure reemerges and the macroscopic polarization appears in the new direction, inverting the sign of Γ . To restore the initial state of P_s , the sign of the external field has to be changed again. Naturally, the scattering pattern will follow all changes in the spontaneous polarization and replicate the spatial evolution of P_s . Thus, the polarization hysteresis will result in a scattering hysteresis, as proven in our experiment when the external field is applied using Procedure 1.

The different values of E_c found on the descending (left) and the ascending (right) parts of the m_s - E hysteresis can be attributed to the memory effect appearing in the field-cooled samples. During the poling procedure described in Sect. 2, strong internal fields are induced in the crystal volume at high temperatures by the external field E_o and then frozen during the cooling process. These fields cause a predisposition of the macroscopic polarization to assume its initial orientation if the crystal is then repeatedly repoled by an alternating external field at low temperature. A similar memory effect has been observed in measurements of the ferroelectric hysteresis [19].

If the same experiment is performed using Procedure 2, where the external field is applied on the illuminated crystal, it does not reproduce the above results (see Fig. 5). This differing behavior can be explained as follows: since the crystal is illuminated incompletely (the beam diameter is smaller than the dimensions of the entrance face of the crystal), photoexcited electrons drifting in the external field are captured on the beam borders, causing an excess of negative charges on the beam edge closer to the '+'-charged side of the crystal, and of positive charges on the beam edge closer to the '-'-charged side. The resulting internal macroscopic field can screen the illuminated area of the crystal from the external field if the applied field grows in amplitude slower than the internal field. The speed of this screening is determined by the photoinduced conductivity. Since in Procedure 2 the voltage jump between two successive scans is too small for an immediate domain inversion, the light-induced screening field is able to compensate the external field and to hinder domains from spatial switching.

Additional experiments show that the successful spatial inversion of a beam-fanning profile with Procedure 2 is possible only if the external field is applied instantaneously with an amplitude E_o much higher than E_c . Thus, the incomplete illumination of a ferroelectric crystal at slowly varying external fields $E_o < E_c$ can be an effective tool for locking the orientation of the spontaneous polarization and to avoid the

reversal of the orientation of domains in the illuminated area even under a field $E_o > E_c$.

From the general relation (2) between the linear electrooptic effect and the spontaneous polarization of a photorefractive crystal, we have shown qualitatively that the light-induced scattering hysteresis is unambiguously defined by the relevant P_s - E hysteresis. Quantitative consideration of this question requires further development of the model of photorefractive scattering, and particularly a separate study of the origin of the seed scattering (primary scattering I_{so}) and the subsequent process of nonlinear amplification (gain coefficient Γ) of the scattered light. I_{so} and Γ are two independent parameters defining the intensity distribution of the scattering. Most papers about light-induced scattering in photorefractive crystals have focused on the process of light amplification and almost never discuss deeply the question of the origin and the properties of this primary scattering. In the next section, we will try to fill this gap at least for the case of a SBN crystal.

4.3 Seed scattering and gain coefficient versus polar structure of SBN

To complete the study of beam-fanning in SBN, we shall discuss the seed scattering I_{so} itself and the effect of the external field and optical illumination on the scattering sources. The relationship between the coefficient Γ and the scattering angle θ_s is given in (1). It can be expected that the seed intensity I_{so} is not spatially uniform. Moreover, we will show that it depends on the external field E_o too.

We apply the following model for seed scattering in a SBN:Ce crystal: the polar structure in the crystal can be considered to be composed of different periodic and/or quasi-periodic assemblies of domains distributed in the bulk and aligned along the c axis. The existence of such bulk domains has been proven in SBN by Fogarty et al. [12]. Their size and arrangement are a fingerprint of the pretreatment of the crystal, and lead to a specific macroscopic polarization [30]. Obviously, the internal random fields postulated in the random-field Ising model for the explanation of the relaxor-like phase transition in SBN [31, 32] should also play a decisive role in the formation of a rich domain structure. We therefore assume that numerous domains are present even in SBN crystals with the maximum macroscopic polarization. We further assume that the largest contribution to the initial optical noise is due to diffraction of the pump beam on optical inhomogeneities located on boundaries of ferroelectric domains. Local depolarizing fields concentrated on these boundaries yield local perturbations Δn of the index of refraction, caused by the linear electrooptic effect. They are built-in, along with the domain structure, and remain unchanged if the crystal is not exposed to external influences like thermal treatment, optical illumination, application of external fields, etc. The most efficient modulations of the refractive index appear in the $\pm c$ -directions, because r_{33} is the largest electrooptic coefficient. Large-scale domains with larger P_s cause higher fields than small domains, resulting in larger amplitudes of Δn . The scattering properties of such built-in perturbations depend strongly on their spatial regularity, whereby the most efficient scattering occurs if the perturbations are arranged with high regularity. Any deviation or a low spatial regularity will lead to a decrease of

the scattered intensity. The diffraction of the pump beam on the Δn -perturbations associated with the large-scale domain structures results in small-angle seed scattering, while Δn -perturbations on assemblies composed of smaller domains result in seed components propagating at larger θ_s angles. Illumination of the crystal excites free electrons into the conduction band, which should modify the internal fields and affect the corresponding local Δn -structures, enhancing some and weakening others. Instead, the influence of large-scale space-charge fields induced by the interference of the pump and scattered waves on the small-scale structures can be neglected. These space-charge fields do not exceed a few V/cm and are much smaller than the stepwidth ΔE_o used to increase the externally applied electric field.

Since the symmetry properties of SBN cause the alignment of polar domains either along the $-z$ - or the $+z$ -direction, we assume that the angular distribution of the seed scattering in these directions is symmetric. This assumption makes it possible to extract the angular distribution of the gain factor and the seed scattering along the c axis from the corresponding intensity profile (see Fig. 2b). As follows from (1), if the seed intensities for two symmetric scattering angles θ_s and $-\theta_s$ are equal, ($I_{so}^{+\theta_s} = I_{so}^{-\theta_s} = I_{so}^{\theta_s}$), the corresponding gain coefficients Γ differ only in sign ($\Gamma^{+\theta_s} = -\Gamma^{-\theta_s}$), and simple multiplication of the scattering intensities, $I_s^{+\theta_s}$ and $I_s^{-\theta_s}$, should give the value of $I_{so}^{\theta_s}$:

$$I_{so}^{\theta_s} = \sqrt{I_s^{+\theta_s} I_s^{-\theta_s}}. \quad (3)$$

The natural logarithm of the ratio of these intensities gives the value of Γ

$$|\Gamma^{\theta_s}| = \frac{1}{2d} \left(\frac{I_s^{-\theta_s}}{I_s^{+\theta_s}} \right). \quad (4)$$

Applying the procedure given by (3) and (4) to the results of our scattering hysteresis experiment, we obtain the gain coefficient Γ and the seed scattering amplitude I_{so} as functions of the scattering angle θ_s (Fig. 6). The latest results obtained from the study of the temperature properties of beam-fanning [30] show that the above procedure works properly in the temperature range $T < T_c$: fitting of the angular Γ -dependencies using (1) gives values for the electrooptic coefficient r_{33} and the effective trap density N_{eff} identical to those obtained from other experiments.

Now we can draw some conclusions about the effect of an external field and coherent illumination on the domain structure in SBN by analyzing the experimental results with respect to our model of seed scattering.

The angular distributions of Γ and I_{so} for the values $E_o = 0, -1.3, -1.5, -1.8,$ and -4 kV/cm, marking the key points in the scattering hysteresis, were extracted from the corresponding experimental curves in Fig. 3 and are shown in Fig. 6a for Γ and Fig. 6b for I_{so} . Similar to the intensity I_s in Fig. 3, the intensity I_{so} in Fig. 6 is normalized relative to the pump beam intensity I_p^{max} . For easier identification, the curves in Fig. 6 are labeled identically to the corresponding curves in Fig. 3. The comparison between Fig. 6a and Fig. 3 reveals a correspondence between the Γ - and I_s -curves: 1) At external fields smaller than the coercive field ($E_o < E_c$), the Γ -curve

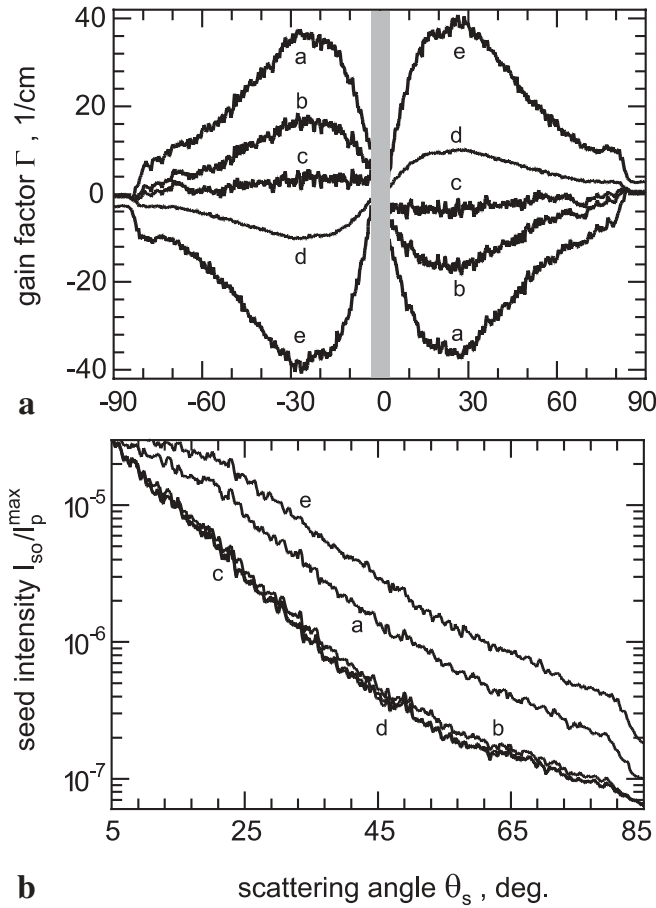


FIGURE 6 Angular distribution of the gain factor Γ (a) and the normalized seed intensity $I_{so}/I_p^{E=0}$ (b) calculated for different values of E_0 from corresponding light intensity scans shown in Fig. 3. The central *shadowed area* corresponds to the angular interval influenced by the transmitted pump beam

shows positive values on the left hand side, where the scattering intensity I_s is much higher, and negative values on the right hand side, where the scattering intensity is much lower; 2) At $E_0 \approx E_c$, the absolute values of Γ and I_s decrease, and the I_s -curve becomes symmetric, while the Γ -curve flattens; 3) For $E_0 > E_c$, the left and right hand sides of the Γ -curve and the I_s -curve switch places. All these features indicate that at $E_0 = E_c$ the domain structure in SBN is mostly disordered, that for $E_0 > E_c$ the long-range order restores itself in the new direction and the macroscopic polarization of the crystal increases again, and that for $E_0 \gg E_c$ most of the domains are aligned along E_0 , and P_s reaches a maximum here.

Distinct from the I_s -curves, the angular distribution of I_{so} for $E_0 = -(1.3 \div 1.8)$ kV/cm is stable. It increases only if E_0 is far from E_c . One can see from Fig. 6b, that except at small scattering angles the curves a and c are nearly parallel, while at small angles they seem to converge. This indicates that large domains (causing large-scale Δn -structures and small θ_s angles) suffer less disordering at $E_0 = E_c$ than small domains, which cause small-scale Δn -structures and large θ_s angles.

The dependencies of Γ and $I_{so}/I_p^{E=0}$ (where $I_p^{E=0}$ is taken at $E_0 = 0$ kV/cm) on the field E_0 are shown in Fig. 7a for Γ and Fig. 7b for $I_{so}/I_p^{E=0}$ for two different scattering angles $\theta_s = 15^\circ$ and 50° . These angles correspond to spatial structures with periods $\Lambda = 2.4 \mu\text{m}$ and 800 nm , respectively. The compar-

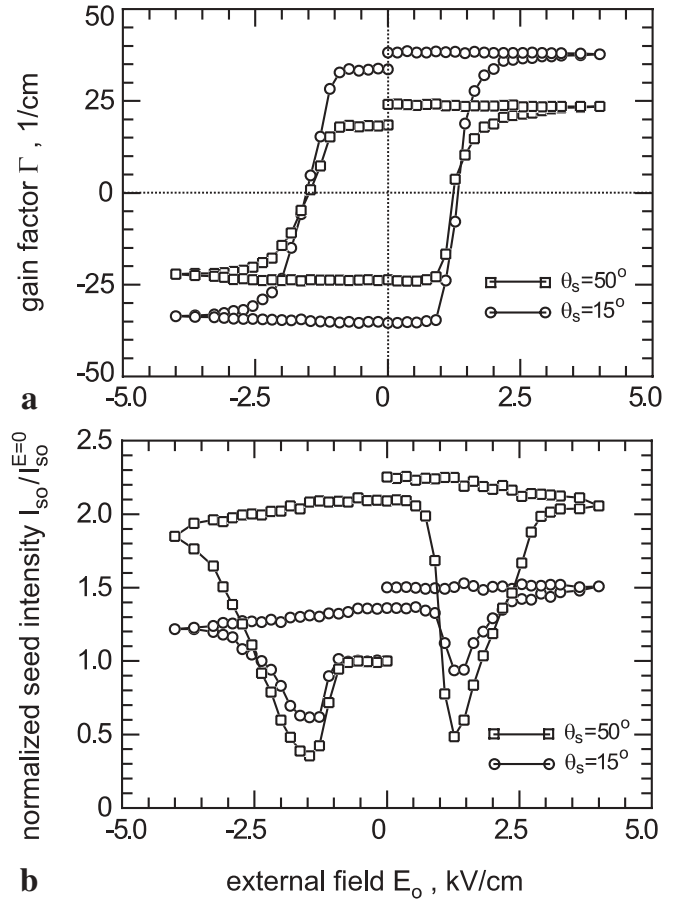


FIGURE 7 Dependence of the gain factor Γ (a) and the normalized seed scattering intensity $I_{so}/I_p^{E=0}$ (b) versus the external field E_0 for two scattering angles: $\theta_s = 15^\circ$ (curve marked by circles) and $\theta_s = 50^\circ$ (curves marked by rectangles)

ison of Figs. 4a and 7a clearly illustrates a direct relation between the scattering hysteresis and the Γ - E hysteresis. Since the Γ - E hysteresis is caused by the P_s - E hysteresis, the scattering hysteresis m_s - E also originates from the P_s - E hysteresis. The different values of E_c measured on the descending (left) and the ascending (right) parts of the Γ - E hysteresis (as well as in the case of m_s - E curve) are attributed to the memory effect discussed in the Sect. 4.2.

The dependence of the seed scattering intensity I_{so} on the external field (see Fig. 7b) exhibits two minima near the external field where Γ approaches zero. This sharp drop in I_{so} is also caused by the domain disordering at $E_0 = E_c$. Incomplete domain reversal at $E_0 = E_c$, and redistribution of photoelectrons to new locations during the subsequent illumination, break the spatial order in the structure of the local fields, and consequently in the Δn -structures. This distortion of the built-in noisy gratings results in a strong decrease of the seed scattering. When the long-range order reemerges at $E_0 > E_c$, it causes a new order for the Δn -structures with respect to the modified spatial alignment of domains. According to Fig. 7b, multiple repetitions of Procedure 1, i.e. repeated coherent illumination of the crystal with subsequent applications of an external field, result in a considerable increase of the seed scattering. This can be explained as follows: an accumulation of photoexcited electrons at the positive tips of

domains, and a corresponding depletion of electrons at the negative tips, results in an increase of the local charges located on these domains and in an enhancement of the Δn -structures. A drain of electric carriers under the external field along domain walls to domain tips yields further changes in local fields. Such a redistribution of electric charge in the crystal volume induced by the coherent illumination also reduces anomalously oriented local fields that are responsible for the existence of 180° -domains, and should assist the further reversal of the 180° -domains, resulting in a refinement of the polar structure in SBN. The last factor also leads to an increase in P_s and Γ .

Therefore, besides electrical treatment, photoexcited charge carriers play an important role during recording of the optical hysteresis. In order to study this influence, it is a decisive experimental requirement that illumination be performed after a steady state of P_s is reached after applying an external electric field E_o , and in addition, that scattered light is detected in the steady state of the light scattering process. Both requirements were met in our experiment. To get a quantitative measure of the influence of photoexcited charge carriers on the spatial alignment of domains we can now define $m_\Gamma = \Gamma_2/\Gamma_1$ as the ratio of the Γ -values at the opening and closing points on the Γ - E hysteresis, and $m_{I_{so}} = I_{so2}/I_{so1}$ as the ratio of I_{so} -values at the opening and closing points on the I_{so} - E dependence. According to (1) and (2), Γ is proportional to P_s , so the ratio m_Γ measures the relative number of 180° -domains switched with the help of the external field and the coherent illumination. The m_Γ ratio for two angles $\theta_s = 50^\circ$ and $\theta_s = 15^\circ$ equals 1.4 and 1.1, respectively. The corresponding values of the $m_{I_{so}}$ ratio are 2.2 and 1.5. Following our assumption that 180° -domain reversal changes Γ and I_{so} alike, the observed simultaneous increase of m_Γ and $m_{I_{so}}$ with increasing scattering angle θ_s shows that smaller domains are switched more effectively than larger domains. Figure 8 shows m_Γ and $m_{I_{so}}$ as functions of the spatial period Λ of the Δn -structures. The curves are limited on the left hand side by the smallest spatial period, corresponding to the largest scattering angle $\theta_s = 90^\circ$ in air, and on the right hand side by the largest spatial period, corresponding to the limiting angle $\theta_s = 5^\circ$, where the influence of the pump beam intensity on the measured signal becomes noticeable. When comparing the absolute values of m_Γ and $m_{I_{so}}$, one has to take into account that an increase of the gain coefficient is attributed to the increase of the macroscopic polarization P_s and depends mostly on the number of switched 180° -domains, while the increase of the seed scattering is attributed to two factors: 1) an improvement of the spatial ordering in local Δn -structures due to a reorientation of 180° -domains; and 2) an increase of the amplitude of the Δn -structures due to the increase of r_{33} in ferroelectrics with refined domain alignment and due to the additional charge accumulation at the domain borders by photoexcited electrons. We also should point out that the angular profiles measured in the transmitted light give information only about structures with spatial dimensions in the range 0.6 to 7.3 μm . To study objects of smaller scale, one has to expand the angular range by measuring the scattering distribution of the reflected light.

Therefore, besides electrical treatment, photoexcited charge carriers play an important role during recording of the optical hysteresis. In order to study this influence, it is a decisive experimental requirement that illumination be performed after a steady state of P_s is reached after applying an external electric field E_o , and in addition, that scattered light is detected in the steady state of the light scattering process. Both requirements were met in our experiment. To get a quantitative measure of the influence of photoexcited charge carriers on the spatial alignment of domains we can now define $m_\Gamma = \Gamma_2/\Gamma_1$ as the ratio of the Γ -values at the opening and closing points on the Γ - E hysteresis, and $m_{I_{so}} = I_{so2}/I_{so1}$ as the ratio of I_{so} -values at the opening and closing points on the I_{so} - E dependence. According to (1) and (2), Γ is proportional to P_s , so the ratio m_Γ measures the relative number of 180° -domains switched with the help of the external field and the coherent illumination. The m_Γ ratio for two angles $\theta_s = 50^\circ$ and $\theta_s = 15^\circ$ equals 1.4 and 1.1, respectively. The corresponding values of the $m_{I_{so}}$ ratio are 2.2 and 1.5. Following our assumption that 180° -domain reversal changes Γ and I_{so} alike, the observed simultaneous increase of m_Γ and $m_{I_{so}}$ with increasing scattering angle θ_s shows that smaller domains are switched more effectively than larger domains. Figure 8 shows m_Γ and $m_{I_{so}}$ as functions of the spatial period Λ of the Δn -structures. The curves are limited on the left hand side by the smallest spatial period, corresponding to the largest scattering angle $\theta_s = 90^\circ$ in air, and on the right hand side by the largest spatial period, corresponding to the limiting angle $\theta_s = 5^\circ$, where the influence of the pump beam intensity on the measured signal becomes noticeable. When comparing the absolute values of m_Γ and $m_{I_{so}}$, one has to take into account that an increase of the gain coefficient is attributed to the increase of the macroscopic polarization P_s and depends mostly on the number of switched 180° -domains, while the increase of the seed scattering is attributed to two factors: 1) an improvement of the spatial ordering in local Δn -structures due to a reorientation of 180° -domains; and 2) an increase of the amplitude of the Δn -structures due to the increase of r_{33} in ferroelectrics with refined domain alignment and due to the additional charge accumulation at the domain borders by photoexcited electrons. We also should point out that the angular profiles measured in the transmitted light give information only about structures with spatial dimensions in the range 0.6 to 7.3 μm . To study objects of smaller scale, one has to expand the angular range by measuring the scattering distribution of the reflected light.

5 Conclusions

Light-induced scattering (beam-fanning) has been studied in detail in photorefractive SBN:Ce (0.66 mol %) under various external electric fields E_o . The optical hysteresis in the scattering was observed and interpreted as being the result of the P_s - E hysteresis. The properties of the scattering were analyzed with respect to changes in the domain structure of the crystal induced by the appropriate action of external fields and coherent illumination. A model of seed scattering in SBN is proposed and corroborated by the experimental results. It is shown that the successive application of coherent light and electric field to the crystal improves the domain structure, enhances the photorefractive amplification, and modifies the scattering centers in the crystal.

Finally, we conclude that the study of beam-fanning and seed scattering can be a powerful tool for obtaining detailed information about the polar structure in SBN.

ACKNOWLEDGEMENTS This work was supported by the Deutsche Forschungsgemeinschaft within the framework of the Schwerpunktprogramm SPP 1056: 'Strukturgradienten in Kristallen' (Project WO 618/3-3) and INTAS Project 01-0173. M.G. acknowledges support from the DFG for his stay in the Institut für Mineralogie, Universität zu Köln.

REFERENCES

- 1 V.V. Voronov, E.H. Gulanyan, I.R. Dorosh, Y.S. Kuzminov, A.L. Mikaelyan, V.V. Osiko, N.M. Polozkov, A.M. Prokhorov: *Sov. J. Quantum Electron.* **6**, 1993 (1979)
- 2 M.D. Ewbank, R.R. Neurgaonkar, W.K. Cory, J. Feinberg: *J. Appl. Phys.* **62**, 407 (1987)
- 3 N.V. Kukhtarev, V.P. Markov, S.G. Odoulov, M.S. Soskin, V.L. Vinetskii: *Ferroelectr.* **22**, 961 (1979)
- 4 S.G. Odoulov, M.S. Soskin, A.I. Khyzniak: *Dynamic Grating Lasers* (Harwood, London 1991)
- 5 J. Feinberg: *J. Opt. Soc. Am.* **72**, 46 (1982)
- 6 A.M. Prokhorov, Y.S. Kuzminov: *Ferroelectric Crystals for Laser Radiation Control* (Adam Hilger, Bristol, Philadelphia, New York 1990)
- 7 Y. Tomita: *Opt. Mater.* **4**, 281 (1995)
- 8 T. Volk, T. Woike, U. Doerfler, R. Pankrath, L. Ivleva, M. Woehlecke: *Ferroelectr.* **203**, 457 (1997)
- 9 V. Grubsky, S. McCormack, J. Feinberg: *Opt. Lett.* **21**, 6 (1991)

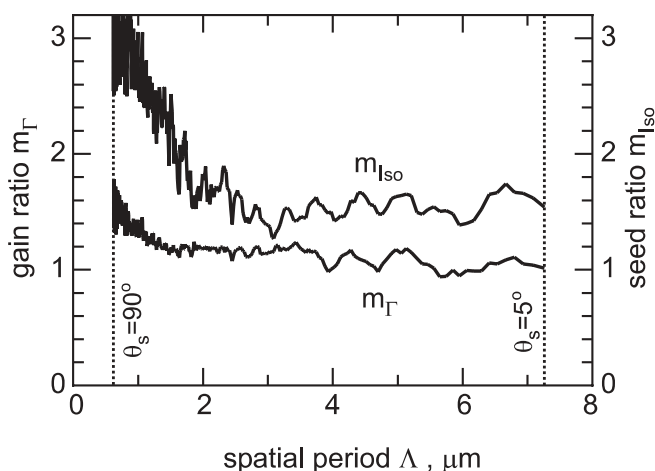


FIGURE 8 Dependence of the gain ratio m_Γ and seed ratio $m_{I_{so}}$ on the spatial dimension Λ

- 10 T. Granzow, U. Dörfler, T. Woike, M. Wöhlecke, R. Pankrath, M. Imlau, W. Kleemann: *Europhys. Lett.* **57**, 597 (2002)
- 11 T. Woike, G. Weckwerth, H. Palme, R. Pankrath: *Solid State Commun.* **102**, 743 (1997)
- 12 G. Fogarty, B. Steiner, M. Cronin-Golomb, U. Laor, M.H. Garrett, J. Martin, R. Uhrin: *J. Opt. Soc. Am. B* **13**, 2636 (1996)
- 13 M.E. Lines, A.M. Glass: *Principles and Applications of Ferroelectrics and Related Materials* (Oxford University Press, London 2000)
- 14 A.V. Knyaz'kov, N.M. Kozhevnikov, Y.S. Kuzminov, N.M. Polozkov, A.S. Saikin, S.A. Sergushenko: *Sov. Tech. Phys. Lett.* **9**, 171 (1983)
- 15 J. Ma, L. Liu, S. Wu, L. Xu, B. Shu: *Appl. Phys. Lett.* **53**, 826 (1988)
- 16 T. Woike, T. Volk, U. Dörfler, R. Pankrath, L. Ivleva, M. Wöhlecke: *Ferroelectr. Lett.* **23**, 127 (1998)
- 17 T. Volk, L. Ivleva, P. Lykov, D. Isakov, V. Osiko, M. Wöhlecke: *Appl. Phys. Lett.* **79**, 854 (2001)
- 18 F. Kahmann, R. Matull, R.A. Rupp, J. Seglins: *Europhys. Lett.* **13**, 405 (1990)
- 19 T. Granzow, U. Dörfler, T. Woike, M. Wöhlecke, R. Pankrath, M. Imlau, W. Kleemann: *Phys. Rev. B* **63**, 174101 (2001)
- 20 M. Gouklov, M. Imlau, R. Pankrath, T. Granzow, U. Dörfler, T. Woike: *J. Opt. Soc. Am. B* **20**, 307 (2003)
- 21 V. Westphal, W. Kleemann, M.D. Glinchuk: *Phys. Rev. Lett.* **68**, 847 (1992)
- 22 W. Kleemann: *Int. J. Mod. Phys. B* **7**, 2469 (1993)
- 23 V.V. Voronov, I.R. Dorosh, Y.S. Kuzminov, N.V. Tkachenko: *Sov. J. Quantum Electron.* **10**, 1346 (1980)
- 24 K. Buse, U. van Stevendaal, R. Pankrath, E. Krätzig: *J. Opt. Soc. Am. B* **13**, 1461 (1996)
- 25 R.A. Vazquez, F.R. Vachss, R.R. Neurgaonkar, M.D. Ewbank: *J. Opt. Soc. Am. B* **8**, 1932 (1991)
- 26 P. Yeh: *Introduction to Photorefractive Nonlinear Optics* (John Wiley, New York 1993)
- 27 U.B. Dörfler, R. Piechatzek, T. Woike, M.K. Imlau, V. Wirth, L. Bohatý, T. Volk, R. Pankrath, M. Wöhlecke: *Appl. Phys. B* **68**, 843 (1999)
- 28 J.R. Oliver, R.R. Neurgaonkar, L.E. Cross: *J. Appl. Phys.* **64**, 37 (1988)
- 29 A.J. Fox: *J. Appl. Phys.* **44**, 254 (1973)
- 30 M. Gouklov, T. Granzow, U. Dörfler, T. Woike, M. Imlau, R. Pankrath, W. Kleemann: *Opt. Commun.* **218**, 173 (2003)
- 31 P. Lehnen, W. Kleemann, T. Woike, R. Pankrath: *Phys. Rev. B* **64**, 224109 (2001)
- 32 T. Granzow, T. Woike, M. Wöhlecke, M. Imlau, W. Kleemann: *Phys. Rev. Lett.* **89**, 127601 (2002)